

Heat Transfer and Flow Characteristics in Vertical Annular Two-Phase Two-Component Flow

Somchai Wongwises and Paisan Naphon

Fluid Mechanics & Turbomachinery Research Laboratory (FUTURE)

Department of Mechanical Engineering,

King Mongkut's University of Technology Thonburi,

91 Suksawas 48 , Bangmod, Radburana,

Bangkok 10140, Thailand

Abstract

Experimental and theoretical results on flow, heat and mass transfer characteristics for the countercurrent flow of air and water in a vertical circular pipe are compared. An experimental setup was designed and constructed. Hot water is introduced through a porous section at the upper end of a test section and flows downward as a thin liquid film on the pipe wall while the air flows countercurrently. The air and water flow rates used in this study are those before the flooding is reached. A developed mathematical model is separated into three parts: A high Reynolds number turbulence model, in which the local state of turbulence characteristics consists of the turbulent kinetic energy (k) and its dissipation rate (ϵ). The transport equations for both k and ϵ are solved simultaneously with the momentum equation to determine the kinetic turbulence viscosity, the pressure drop, interfacial shear stress and then the friction factor at the film/core interface; heat and mass transfer models are proposed in order to estimate the distribution of the temperature and the mass fraction of water vapor in gas core. The results from the model are compared with the present experimental ones. It can be shown from the present study that the influence of the interfacial wave phenomena is significant to the pressure loss, and the heat and mass transfer rates in the gas phase.

1. Introduction

Many of the two phase flow transportation processes found in industrial applications occur in the annular flow regime. Annular two-phase flow is one of the most important flow regimes and is characterized by a phase interface separating a thin liquid film from the gas flow in the core region. Two-phase annular flow occurs widely in film heating and cooling processes, particularly in power generation and especially in nuclear power reactors. This flow regime has received the most attention both analytically and experimentally [1-5] because of its practical importance and the relative ease in which analytical treatment may be applied.

Relatively little information, however, is currently available on the heat and mass transfer characteristics of two-phase countercurrent annular flow in a vertical pipe. Some of earliest work was performed by Suzuki et al. [6]. They proposed a theoretical method to evaluate the heat transfer and flow characteristics of a two-phase, two-component annular flow with a thin film heated at low heat flux. A simple model for the wave effect employed in their study predicts the heat transfer well. Hijikata et al. [7] studied the flow characteristics and heat transfer in countercurrent water and air flows. A theoretical model based on a low Reynolds number k - ϵ turbulence model was proposed, where an additional production term was

considered to incorporate the wave effects. In the present study, the experimental and theoretical data on flow, heat and mass transfer characteristics for the vertical countercurrent annular flow are investigated. The effects of any relevant parameter on pressure loss, and the heat and mass transfer rate are also discussed.

2. Experimental Apparatus and Method

The experimental apparatus is shown schematically in Fig.1. The test section, with an inside diameter of 24 mm and the length of 1.9 m was constructed from transparent acrylic glass to permit visual observation of the flow patterns. The water temperature was raised to the desired level by using electric heaters and was controlled by a temperature controller and then pumped through a rotameter to the water inlet section. The water inlet section was constructed from two concentric tubes, the inner tube being the test section or sinter which was radially drilled with many small holes. The inner tube of the sinter was also covered with a fine wire mesh to distribute the water smoothly along the pipe. The water in the inlet section flowed downwards as a liquid film along the test section while the air flowed countercurrently. The level of water in the water outlet section was kept constant, and the excess water was drained out.

An upper open end condition was used in the experiments. Air was supplied to the test section by a blower and the flow rate was controlled by a valve at the outlet of the blower. The inlet flow rate of air was measured by means of an orifice and micromanometer, and the inlet flow rate of water was measured by a rotameter. The relative humidities of inlet and outlet air were calculated from wet and dry bulb temperatures and were checked by digital humidity meter (electrostatic capacitance type) using a polymer film as a sensor. The water temperatures at three positions along the test section were measured by thermistors. The two phase pressure drop between the test section was measured by a digital manometer. Stainless ring electrodes were mounted flush in the tube wall for measuring the film thickness. The measuring positions were located at 30 cm and 170 cm from the lower end of the test section. They operate on the principle of the variation of

electrical resistance with changes in the water film thickness between two parallel electrode rings. The same description of the calibration procedures for annular flow can be found in Andreussi [8]. Due to the variation of conductivity with temperature and coating of the electrodes with impurities, the gauges were calibrated before and after each run.

Experiments were conducted at various air, water flow rates, and water temperatures. The air flow rate was increased by small increments while the water flow rate at a specific temperature was kept constant. After each change in the inlet air flow rate, both the air and the water flow rates, the relative humidity of air at inlet and outlet of the test section were recorded. The pressure drop across the test section and the film thickness were registered through the transducers and transferred to the data acquisition system. The flow phenomena were also detected by visual observation. The experiments were stopped before the onset of flooding was reached.

3. Mathematical model

In order to compare with the present experimental results, the theoretical model of Hijikata et al. [7] is modified for this study. In the present paper, a model based on a high Reynolds number $k-\epsilon$ turbulence model is proposed. The notation used for the calculation is shown in Fig. 2. The model is separated into three parts; flow, heat and mass transfer characteristics with the following assumptions:

- The gas flow is fully developed because of the large length-to-diameter ratio.
- The effect of vaporization on the gas flow field is neglected.
- Physical properties are constant and independent of the composition.

3.1. Turbulence flow characteristic:

In turbulent flow, velocity fluctuations exchange momentum between adjacent layers of fluid, thereby causing apparent shear stresses that must be added to the stress caused by the mean velocity gradients. For a fully developed turbulent channel flow, the total shear stress is, therefore, given by

$$\tau = \mu \frac{dU}{dy} - \rho \overline{u'v'} \quad (1)$$

The term $-\rho \overline{u'v'}$ is referred to as the turbulent shear stress which is related to the mean rate of strain via a turbulent viscosity (Jones and Launder [9]).ie.

$$-\rho \overline{u'v'} = \mu_t \frac{\partial U}{\partial y} \quad (2)$$

A turbulent viscosity term therefore appears in the present model.

Momentum equation;

$$0 = -\frac{1}{\rho} \frac{dP}{dz} + \frac{1}{r} \frac{\partial}{\partial y} \left(r (U + v_t) \frac{\partial U}{\partial y} \right) \quad (3)$$

Jones and Launder [9] presented turbulence models based on high and low Reynolds numbers in order to predict the laminarization. A high Reynolds number k-ε model is employed in this study.

Turbulent kinetic energy (k) equation;

$$\frac{\partial k}{\partial t} = \frac{1}{r} \frac{\partial}{\partial y} \left(r \left(\frac{v_t}{\sigma_k} \right) \frac{\partial k}{\partial y} \right) + v_t \left(\frac{\partial U}{\partial y} \right)^2 - \varepsilon \quad (4)$$

Turbulent kinetic energy dissipation (ε) equation;

$$\frac{\partial \varepsilon}{\partial t} = \frac{1}{r} \frac{\partial}{\partial y} \left(r \left(\frac{v_t}{\sigma_\varepsilon} \right) \frac{\partial \varepsilon}{\partial y} \right) + C_1 \frac{\varepsilon}{k} v_t \left(\frac{\partial U}{\partial y} \right)^2 - C_2 \frac{\varepsilon^2}{k} \quad (5)$$

Kinetic turbulent viscosity;

$$v_t = C_\mu \frac{k^2}{\varepsilon} \quad (6)$$

The equations contain five adjustable constants C_μ , C_1 , C_2 , σ_k , σ_ε . The standard k-ε model employs values for the constants that are arrived at by comprehensive data fitting for a wide

range of turbulent flows (Versteeg and Malalasekera [10]; Singhal and Spalding [11]):

$$C_\mu = 0.09, C_1 = 1.44, C_2 = 1.92, \sigma_k = 1.0, \sigma_\varepsilon = 1.3$$

The boundary conditions at the interface ($y = 0$) and the center of pipe ($r = 0$) are given as follows :

$$y = 0: U = -U_{lm}, k = 0, \varepsilon = 0 \quad (7)$$

$$r = 0: \frac{\partial U}{\partial y} = \frac{\partial k}{\partial y} = \frac{\partial \varepsilon}{\partial y} = 0 \quad (8)$$

where U_{lm} is the mean velocity of the liquid film obtained from the experiment.

3.2. Heat transfer characteristic:

The distributions of the temperature of the mixture between dry air and water vapor along the upward flow direction is expressed as:

$$U \frac{\partial T}{\partial z} = \frac{1}{r} \frac{\partial}{\partial y} \left(r \left(a + \frac{v_t}{Pr_t} \right) \frac{\partial T}{\partial y} \right) \quad (9)$$

with a boundary condition;

$$y = 0: T = T_i, \omega_v = \omega_{vs} \quad (10)$$

3.3. Mass transfer characteristic:

The distributions of the mass fraction of the mixture between dry air and water vapor along the upward flow direction is also expressed as:

$$U \frac{\partial \omega_v}{\partial z} = \frac{1}{r} \frac{\partial}{\partial y} \left(r \left(D + \frac{v_t}{Sc_t} \right) \frac{\partial \omega_v}{\partial y} \right) \quad (11)$$

with a boundary condition;

$$r = 0: \frac{\partial T}{\partial y} = \frac{\partial \omega_v}{\partial y} = 0 \quad (12)$$

In turbulent flow, there is no universal relationship between the shear stress field and the mean velocity field. Thus, for turbulent flows we are forced to rely on experimental data. The velocity profile for a fully developed turbulent flow through a rough pipe from Pao

[12] is used in the calculation. The friction factor in his equation is replaced by those obtained from the present experiment. The transport equations for both k and ϵ are solved simultaneously with the momentum equation using the finite difference method to determine the kinetic turbulence viscosity, pressure drop, interfacial shear stress and friction factor at film/core interface.

4. Results and discussion

A large number of graphs can be drawn from the result of the study but because of space limitations, only typical results are shown. In the experiment, mean film thicknesses were measured at $Z = 30$ cm and 170 cm. Average values for both mean film thicknesses for various air and water flow rates are given in Fig. 3. The liquid film mass flow rate in this figure is on a per unit width basis in the spanwise direction. As the water flow rate is increased and the air flow rate held constant, the film thickness also increases. It can also be clearly seen that there is a great difference in the mean film thickness between experiments with and without air flow. The mean film thickness at any air flow rate for a specific water flow rate is, however, nearly the same. Figure 4 shows the relationship between the dimensionless turbulent kinetic energy (k^+ , $k/(u_*^3)$) and dimensionless distance from the interface (y^+ , yu_*/ν). The turbulent kinetic energy falls to zero at the interface. As a result of a wavy interface, the turbulent kinetic energy in the region close to the interface, rises monotonically with the distance from the interface to a maximum point and then drops sharply and approaches an equilibrium value. Because the amplitude of the film thickness fluctuation increases slightly with the air flow rate, the turbulent kinetic energy near the interface for higher air flow rate is higher than for lower flow rate.

Figure 5 shows the variation of the interfacial friction factor with the air Reynolds number for typical test conditions. The friction factor for laminar flow and the Blasius correlation for turbulent flow in smooth pipe are also shown in this figure. The velocity gradient at the interface is much larger for turbulent flow

than for laminar flow. This change in velocity profile causes the interfacial shear stress to increase sharply, with the same effect on the interfacial friction factor. The friction factor decreases gradually along the smooth pipe curve. This figure shows also a comparison of friction factors obtained from the model and the experiments. The agreement of this comparison is not bad through the whole range. As a result of the pipe roughness, experimental friction factors for air single phase flow are found to be higher than those from the Blasius correlation. As the water flow rate is increased, larger disturbance waves are formed. The friction factors at higher water flow rates seem, therefore, a little bit higher than those at lower ones. It should be noted that a similar phenomenon can be found in single phase flow in rough walled pipes.

Figure 6 shows the relationship between the mass fraction of water vapor and the air temperature. The saturated line in this figure is based on the saturation vapor pressure of water. A circular point shows the inlet condition of air (dry air and water vapor), and the solid points show the outlet conditions. While the hot water flows down as a film countercurrently with air flow, vaporization occurs at the interface and water vapor from this vaporization will be added to the existing water vapor. Mass fraction of water vapor at the outlet of the test section are, therefore, higher than those of the inlet and also found to be below the saturation line. When the water temperature is higher, the points approach the saturation line. This is confirmed by visual observation that there is an absence of mist (tiny water droplets). However, if the water temperature is high enough, the water vapor from the vaporization is condensed in air stream to form a mist.

Figure 7 shows the relationship between the Nusselt (Nu) number and the value of $RePr^{0.4}$. A complete heat balance was used to calculate the heat transfer coefficient. The equilibrium conditions of air and water film after passing air through falling hot water film for any interval of time can be established by the following energy balance equation:

$$hA\Delta T_{in} + \Delta G C_{p,v} T_{im} + G_{in} C_{p,in} T_{bin} = G_{out} C_{p,out} T_{bout}$$

The first, second, third and fourth term represent heat transferred from the falling water to the air stream, the enthalpy of vapor evaporated from the water film, the enthalpy of the inlet air and the enthalpy of the air leaving the test section respectively. The value of ΔT_{lm} is the log mean temperature difference between both fluids. T_{im} is the mean water temperature at the interface. Consider the Nu number, based on a pipe diameter, rearranged in the form, $Nu = hd_i/\xi$ and the heat transfer coefficient from the energy balance equation, the following equation is obtained;

$$Nu = \frac{d_i (G_{out} C_{p,out} T_{b,out} - G_{in} C_{p,in} T_{b,in} - \Delta G C_{p,v} T_{im})}{\xi (\Delta T)_{lm} \pi d_i L}$$

The latent heat of vaporization is not included because, in this paper, the Nu number is defined for a sensible heat transfer. The figure also shows the effect of the upward air flow on the heat transfer coefficient. At a specific water temperature, the Nu number (or the heat transfer coefficient) increases with increases in the air flow rate. The solid line is the Nu number calculated from Dittus-Boelter equation for fully developed turbulent flow in smooth tubes; $Nu = 0.023 Re^{0.8} Pr^{0.4}$. There is a good agreement here. Any discrepancies are due to the wave formed at the interface and variation of the water temperature along the pipe. Figure 8 shows the relationship between an average temperature ratio and the dimensionless distance from the interface, at $z = 1$ m. At the same inlet water flow rate and temperature, an increase in air flow rate causes a higher fluctuation of the film thickness, and thus higher rate of heat transfer. It corresponds to the results in Fig. 7. The temperature profiles however, differ slightly from each other.

Mass transfer characteristics can be discussed in the same way as those of the heat transfer. Consider the Sherwood (Sh) number = $k_m d_i / D$ in which k_m is the mass transfer coefficient and D is the mass diffusivity. The mass transfer coefficient substituted in this equation is calculated from the mass balance equation and finally the following equation is obtained;

$$Sh = (1 - \omega_{vi}) \frac{d_i}{\rho D (\Delta \omega_v)_{in}} \frac{\Delta G}{\pi d_i L}$$

The results from Figs. 9 and 10 are closely associated with those from Figs. 7 and 8. The relationship between the Sh number and the value of $Re^{0.83} Sc^{0.33}$ is shown in Fig. 9. The similarities between the governing equations for heat, mass, and momentum transfer suggest that the empirical correlations for the mass transfer coefficient would be similar to those for the heat transfer coefficient. This turns out to be the case, and some of the empirical relations for mass transfer from a liquid that completely wets the inside of a tube to a turbulent gas that is flowing is given by Ozisik [13];

$$Sh = 0.023 Re^{0.83} Sc^{0.33}$$

The Sh number at any water flow rate for specific air flow rate and specific water temperature is, however, nearly the same. The solid line in Fig. 9 shows the Sh number calculated from above equation. The Sh number from the experiment is slightly higher than the theoretical value. The difference between them is considered to be a result of the wave formed at the interface. The profiles of mass fraction ratio predicted at $Z = 1$ m are also shown in Fig. 10. At specific water and air flows, the rate of vaporization increases with increases of the water temperature. It should be noted that in the present experiment where mist formation does not occur, the temperature and vapor concentration profiles are almost the same.

5. Conclusions

Experiments have been performed to study the flow, heat and mass transfer characteristics of air-water two-phase countercurrent annular flow in a vertical pipe. A theoretical model has been developed. The model is separated into three parts: a high Reynolds number turbulence model, in which the local state of turbulence characteristics are controlled by the turbulence kinetic energy (k) and its dissipation rate (ϵ); and the heat and mass transfer models. The transport equations for both k and ϵ are solved simultaneously with the momentum equation to

determine the kinetic turbulence viscosity, the pressure drop, interfacial shear stress and then, the friction factor at the film/core interface. The distribution of the temperature and the mass fraction of water vapor in the gas core is also estimated from the heat and mass balance equations, and the kinetic turbulence viscosity is obtained from the former step. The results from the model are in reasonable agreement with the experimental results. It was found that the interface is often wavy in nature and the influence of the interfacial wave is of significance on the momentum, heat and mass transfer characteristics.

Acknowledgments

The present study was supported financially by the Thailand Research Fund (TRF) whose guidance and assistance are gratefully acknowledged. The authors would like to express their appreciation to Professor Takao Nagasaki from Tokyo Institute of Technology for the valuable answers on the subject.

Nomenclature

a	thermal diffusivity, m^2/s
A	heat transfer area, m^2
C_1, C_2 and C_μ	constant in Eqs.(5) and (6)
C_p	specific heat, $J/kg \text{ } ^\circ C$
C_f	friction factor
d	pipe diameter, m
d_j	diameter of gas core, m
D	mass diffusivity, m^2/s
G	mass flow rate, kg/s
h	heat transfer coefficient, $W/m^2 \text{ } ^\circ C$
k	turbulent kinetic energy, m^2/s^2
k^+	dimensionless turbulent kinetic energy
k_m	mass transfer coefficient, m/s
L	pipe length, m
Nu	Nusselt number
P	pressure, N/m^2
Pr	Prandtl number
r	radial distance coordinate
Re	Reynolds number
Sc	Schmidt number
R_j	distance from the pipe centerline to the interface, m
Sh	Sherwood number
t	time
T	temperature, $^\circ C$

U	mean velocity, m/s
u_*	friction velocity, $m/s (= (\tau_i / \rho)^{1/2})$
u', v'	fluctuating components of velocity, m/s
$\overline{u'v'}$	time average of the product of u' and v'
y	distance from the air-water interface, m
y^+	dimensionless distance ($= yu_* / \nu$)
z	distance from the bottom of the test section, m

Greek Symbols

ρ	density, kg/m^3
$\sigma_k, \sigma_\epsilon$	constant in Eqs. (4) and (5)
τ	shear stress, N/m^2
ν	kinematic viscosity, m^2/s
μ	dynamic viscosity, kg/sm
Δ	difference
ϵ	turbulent kinetic energy dissipation, m^2/s^3
ω	mass fraction
ξ	thermal conductivity, W/mC
δ	liquid film thickness, m

Subscripts

b	bulk
c	value at the centerline of the pipe
g	air
i	interface
in	inlet
l	liquid
ln	log mean difference
m	mean value
out	outlet
t	turbulent
v	water vapor
vs	saturated vapor

6. References

- [1] Azzopardi, B.J. and Williams, N.M. (1980), *Multi-Phase Transport*, McGraw-Hill, New York.
- [2] Fore, L.B. (1995), *Int. J. Multiphase Flow*, Vol. 21, p. 137 .
- [3] Joseph, D.D. and Bannwart, A.C. (1996), *Int. J. Multiphase Flow*, Vol. 22, p. 1247.
- [4] Wolf, A., Jayanti, S. and Hewitt, G.F. (1996), *Int. J. Multiphase Flow*, Vol. 22, p. 325.

- [5] Ghiaasiaan, S.M., Wu, X ., Sadowski, D.L. and Abdel-Khalik, S.I. (1997), *Int. J. Multiphase Flow*, Vol. 23, p. 1063.
- [6] Suzuki, K., Hagiwara, Y. and Sato, T. (1983), *Int. J. Heat Mass Transfer*, Vol. 26, p. 597.
- [7] Hijikata, K., Nagasaki, T., Yoshioka, J. and Mori, Y. (1988), *JSME International Journal*, Vol. 31, p. 429.
- [8] Andreussi, P., Di Donfrancesco, A. and Messia, M. (1988), *Int.J.Multiphase Flow*, Vol. 14, p. 777.
- [9] Jones, W.P. and Launder, B.E. (1972), *Int.J. Heat Mass Transfer*, Vol. 15, p. 301.
- [10] Versteeg, H.K. and Malalasekera, W. (1995), *An Introduction to Computational Fluid Dynamics*, 1st ed., Longman, London.
- [11] Singhal, A.K. and Spalding, D.B. (1981), *Computer Methods in Applied Mechanics & Eng.*, Vol. 25, p. 365.
- [12] Pao, R.H.F. (1961), *Fluid Mechanics*, Wiley, New York .
- [13] Ozisik, M. (1985), *Heat Transfer*, McGraw-Hill, New York.

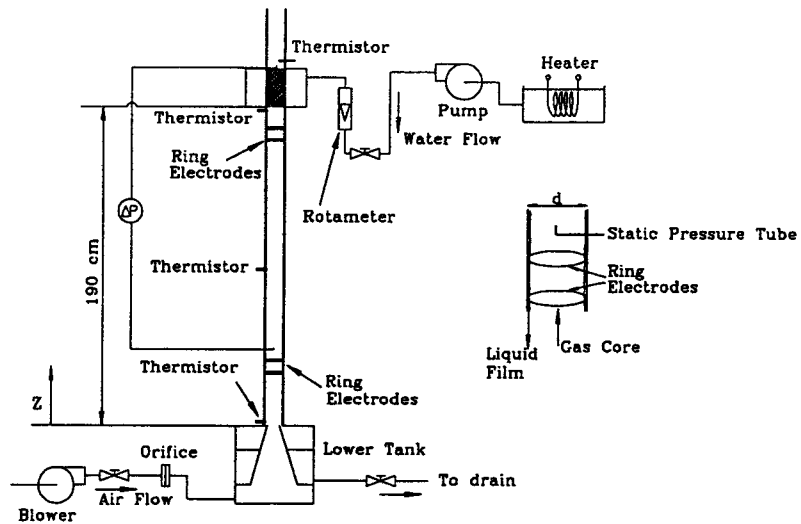


Figure 1. Schematic diagram of experimental apparatus

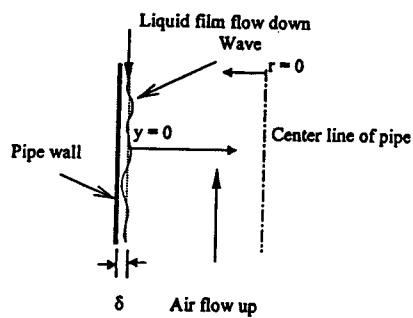


Figure 2. Geometry of annular flow

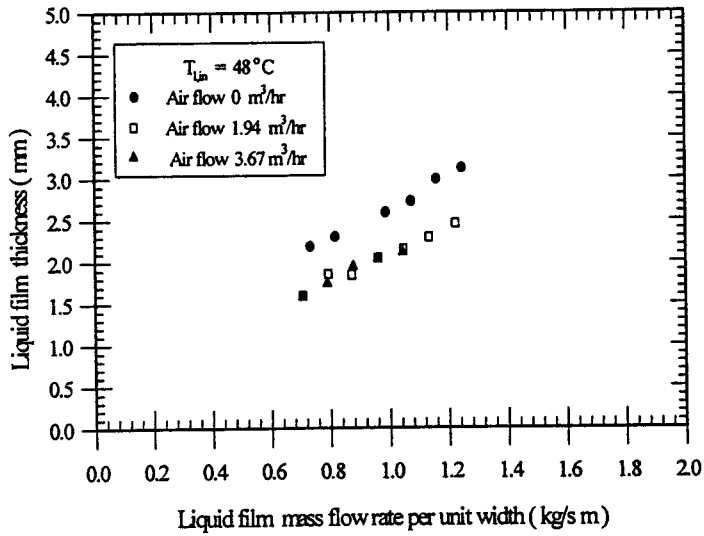


Figure 3. Plot of film thickness against mass flow rate

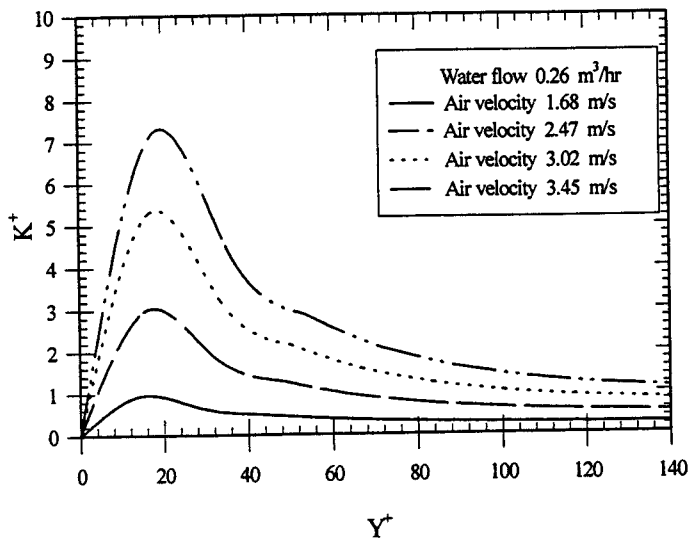


Figure 4. Fully developed kinetic energy profiles

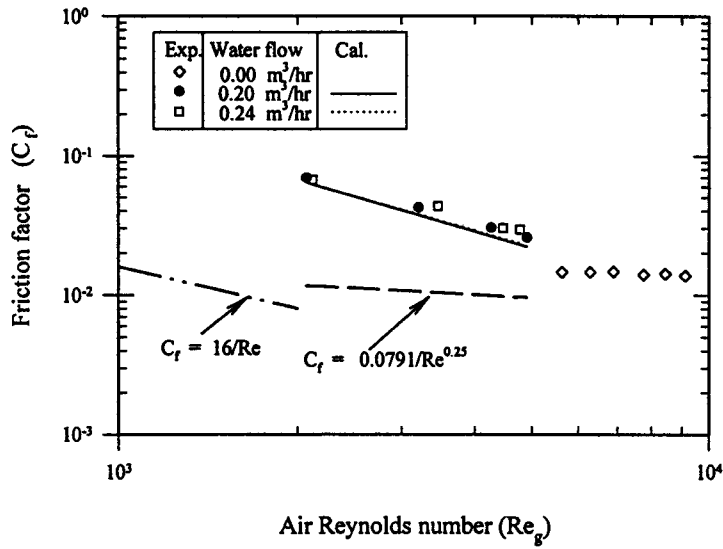


Figure 5. Plot of friction factor against Reynolds number

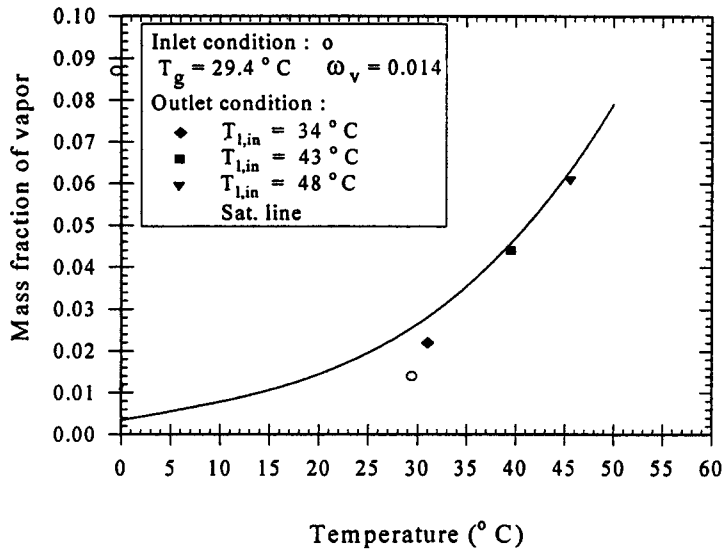


Figure 6. Plot of mass fraction against temperature

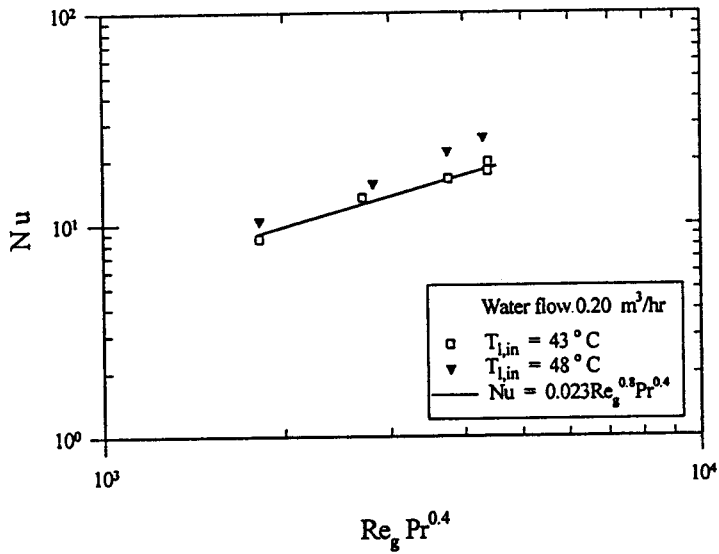


Figure 7. Plot of Nu against $Re_g Pr^{0.4}$

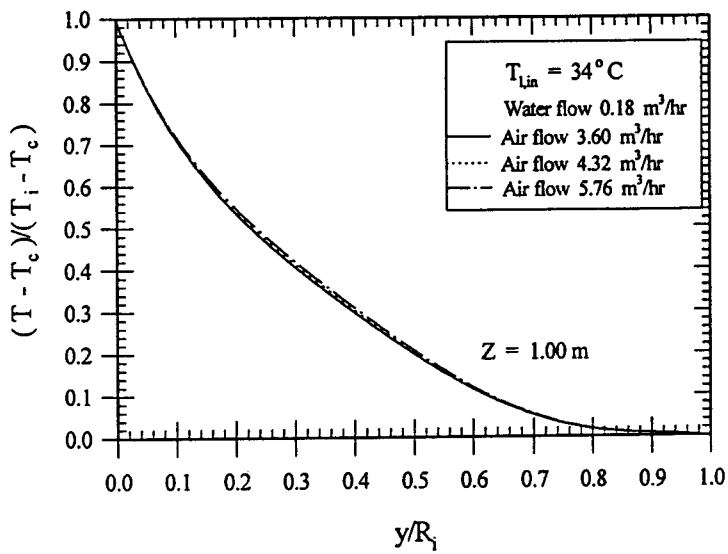


Figure 8. Fully developed temperature profiles

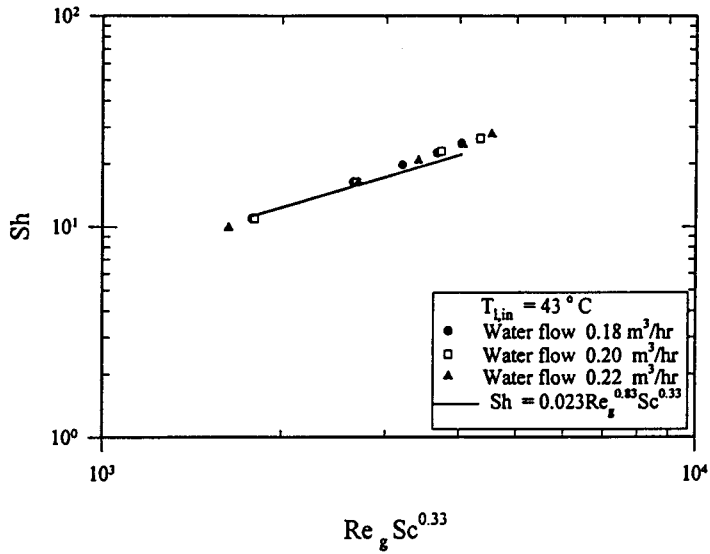


Figure 9. Plot of Sh against $Re_g Sc^{0.33}$

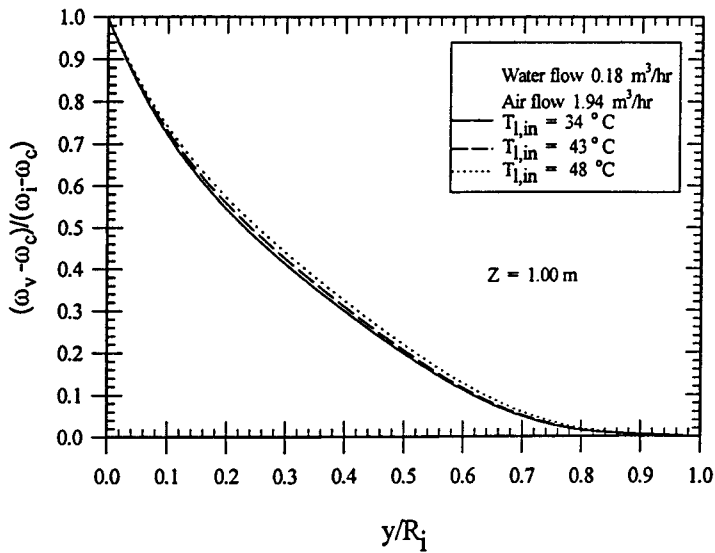


Figure 10. Fully developed mass fraction profiles